Stem Cell Reports
Article

ISSCR

OPEN ACCESS

SETD4 cells contribute to brain development and maintain adult stem cell reservoir for neurogenesis

Sun-Li Cai,[1] Yao-Shun Yang,[1] Yan-Fu Ding,[1] Shu-Hua Yang,[1] Xi-Zheng Jia,[1] Yun-Wen Gu,[1] Chris Wood,[1] Xue-Ting Huang,[1] Jin-Shu Yang,[1] and Wei-Jun Yang[1,2,*]

[1]MOE Laboratory of Biosystem Homeostasis and Protection, College of Life Sciences, Zhejiang University, Hangzhou 310058, China
[2]Laboratory for Marine Biology and Biotechnology, Qingdao National Laboratory for Marine Science and Technology, Qingdao 266000, China
*Correspondence: w_jyang@zju.edu.cn
https://doi.org/10.1016/j.stemcr.2022.07.017

SUMMARY

Cellular quiescence facilitates maintenance of neural stem cells (NSCs) and their subsequent regenerative functions in response to brain injury and aging. However, the specification and maintenance of NSCs in quiescence from embryo to adulthood remain largely unclear. Here, using Set domain-containing protein 4 (SETD4), an epigenetic determinant of cellular quiescence, we mark a small but long-lived NSC population in deep quiescence in the subventricular zone of adult murine brain. Genetic lineage tracing shows that SETD4$^+$ cells appear before neuroectoderm formation and contribute to brain development. In the adult, conditional knockout of *Setd4* resulted in quiescence exit of NSCs, generating newborn neurons in the olfactory bulb and contributing to damage repair. However, long period deletion of SETD4 lead to exhaustion of NSC reservoir or SETD4 overexpression caused quiescence entry of NSCs, leading to suppressed neurogenesis. This study reveals the existence of long-lived deep quiescent NSCs and their neurogenetic capacities beyond activation.

INTRODUCTION

Adult neural stem cells (NSCs) residing within the subventricular zone (SVZ) of the lateral ventricles and the subgranular zone (SGZ) of the hippocampus are known for their ability to generate new neurons that contribute to complex sensory and cognitive functions throughout the lifetime of mammals (Bond et al., 2015; Choi et al., 2018; Doetsch et al., 1999; Mobley et al., 2014; Seri et al., 2001). In the mature brain, these NSCs exist in either a quiescent or an active state (Furutachi et al., 2015; Lugert et al., 2010; Ming and Song, 2011). The state of quiescence has been considered to contribute to long-term maintenance of a reservoir of NSCs by preventing the exhaustion of their proliferation potential and permitting the avoidance of accumulation of damage to DNA, proteins, and mitochondria that might otherwise result in malignant transformation or senescence (Audesse et al., 2019; Cameron et al., 2019; Prozorovski et al., 2008). Upon aging, the higher fraction of NSCs identified in a quiescence state suggests a compensatory mechanism to avoid full depletion of the NSC compartment (Kalamakis et al., 2019). After brain injury, quiescent NSCs can be activated to produce multiple types of progenies to contribute to brain repair (Faiz et al., 2015; Llorens-Bobadilla et al., 2015; Otsuki and Brand, 2020; Delgado et al., 2021). Because of the overall heterogeneity of the NSC population and the lack of defining makers of NSCs that occur in a quiescent state, it is currently unknown how quiescent NSCs originate in the embryo. Their specification and maintenance in adulthood and into old age also remains unclear. Understanding of how quiescent NSCs react in the injured or aged brain and any related potential for therapeutic contributions toward regeneration in the human brain would represent significant advances.

Systemic and local signals seem to regulate NSC quiescence by modulating the expression or function of molecules acting within stem cells. These include transcription factors, cell cycle regulators, and metabolites, which in turn control NSC quiescence or activation (Cavallucci et al., 2016; Kippin et al., 2005; Knobloch et al., 2017; Sueda et al., 2019). Although several molecular players in the regulation of NSC quiescence have been reported (Ahn and Joyner, 2005; Chavali et al., 2018; Engler et al., 2018; Ganapathi et al., 2018; Kandasamy et al., 2014; Marqués-Torrejón et al., 2021; Sueda et al., 2019; Urbán et al., 2019), we know remarkably little about the direct determinants of quiescence and the mechanisms of the transition between active and quiescent states in NSCs.

Epigenetic studies have shown that factors such as chromatin remodeling and histone modification play critical roles in regulating stem cell behaviors, providing genome-wide transcriptional changes and long-lasting effects for downstream signaling pathways (Yao et al., 2016). As a lysine methyl-transferase of histone, SET domain-containing protein 4 (SETD4) has been reported to play a role in cell proliferation by controlling related gene expressions (Faria et al., 2013; Liao et al., 2021). Our previous report revealed that SETD4 regulates cellular dormancy or deep quiescence by H4K20ME3 catalysis in diapause embryos of *Artemia*, a quiescent model system (Dai et al., 2017). SETD4 was then also found to epigenetically regulate quiescence of cancer stem cells in human breast tumor and C-KIT cells in the murine heart by

facilitating heterochromatin formation via H4K20ME3 (Ye et al., 2019; Xing et al., 2021). Thus, an evolutionarily conserved mechanism of cellular quiescence as modulated by SETD4 was proposed.

In this study, upon confirmation of SETD4 marking of a small NSC population in deep quiescence in the SVZ, we performed identification lineage tracing and conditional knockout and knockin of *Setd4* in mice. We found that SETD4$^+$ cells occurred in the neuroepithelium before neuroectoderm formation, contributed to the brain development in early embryo, and then entered a quiescent state in the late embryo. As a long-lived quiescent NSCs, postnatal SETD4$^+$ cells preserve the stem cell reservoir for retaining their function of neurogenesis over extended periods and, upon activation, are able to function in the repair of the injured olfactory bulb (OB).

RESULTS

SETD4 marks a small population of long-lived quiescent NSCs in the SVZ after birth

To investigate whether SETD4$^+$ cells occur in the stem cell niches of brain, we used RNAscope, an RNA fluorescence *in situ* hybridization technique, to reveal endogenous *Setd4* expression in the adult SVZ and SGZ. Using RNAscope combined with immunostaining analysis we found that a small population of NSCs (GFAP, SOX2, and NESTIN) expressed the *Setd4* gene in the adult (2-month-old) SVZ (Figure 1A). However, we did not observe any *Setd4* expression in the adult SGZ (Figure S1A). We then generated inducible transgenic *Setd4-CreER^{T2}::mTmG* lineage tracing mice in which CreER^{T2} recombinase is under the control of the SETD4 promoter. Upon tamoxifen (TAM) induction, membrane-based green fluorescent protein (GFP) was expressed, allowing endogenous SETD4$^+$ cells to be followed (Figure 1B). Beyond a series of TAM pulses and 3 day chases, RNAscope analysis confirmed that TAM-induced GFP accurately marked SETD4$^+$ cells (Figure 1C). We identified a small population of GFP$^+$ cells (1.78% ± 0.10%) in the SVZ of 2-month-old *Setd4-CreER^{T2}::mTmG* mice (Figure 1D). Consistent with observations using the RNAscope assay, we did not observe any GFP$^+$ cells in the SGZ of the dentate gyrus (Figure S1A). In the SVZ, these GFP$^+$ cells existed along the lateral ventricular wall as single-cell clones and lacked any KI67 or PCNA expression, markers of cell proliferation, indicating that they were in quiescent state (Figure 1E). To confirm this, an EdU incorporation assay was performed. We found that all TAM-induced GFP$^+$ cells were EdU negative (Figure 1E). This was consistent with the former KI67 and PCNA negative data. Moreover, the majority (more than 90%) of GFP$^+$ cells expressed GFAP, SOX2, and NESTIN as NSC markers but lacked any expression of MASH1, DCX, NEUN, or OLIG2, markers of transit-amplifying cells (TAPs), and also lacked any immature migratory neuroblasts (NBs), mature neurons or oligodendrocytes (Figures 1F and S1B). These GFP$^+$ cells exhibited the typical radial morphology of NSCs having minute apical endings to their ventricular surfaces and long basal processes (Figure 1G) (Mirzadeh et al., 2008; Obernier and Alvarez-Buylla, 2019; Delgado et al., 2021). We considered such data as confirmation of the SETD4$^+$ quiescent NSC identity.

To identify whether SETD4$^+$ cells also exist as quiescent NSCs in the aged SVZ, we also analyzed *Setd4* expression in aged (20-month-old) mice by RNAscope. Results showed that the SETD4$^+$ NSCs (GFAP$^+$, SOX2$^+$, and NESTIN$^+$) existed in the SVZ of aged mice (Figure S1C). Similarly, 15-month-old *Setd4-CreER^{T2}::mTmG* mice were induced by TAM (Figure 1B). RNAscope analysis showed that TAM-induced GFP$^+$ cells could still accurately mark SETD4$^+$ cells (Figure S1D). As observed in 2-month-old mice (Figures 1D–1G), a small population of GFP$^+$ cells were also identified as quiescent NSCs in the aged SVZ, occurring along the lateral ventricular wall, showing positive for NSC markers, negative for KI67 expression, and displaying NSC morphology (Figures S1E–S1H). We analyzed the whole-brain sections of 24 h TAM-induced *Setd4-CreER^{T2}::mTmG* mice at early postnatal day (P7), adult (2 months), and aged (20 months) (Figure S1I). We found that SETD4-expressing cells existed only within the wall of the ventricular zone in the forebrain and expressed SOX2 but not KI67 throughout these stages (Figures S1J–S1L). We concluded that SETD4 marks a small population of quiescent NSCs in the SVZ of the mouse brain.

As we observed SETD4$^+$ NSCs existed in the SVZ of neonatal (P3) brain (Figure S2A), to explore SETD4$^+$ NSCs properties after birth, lineage tracing was performed at early postnatal and adult. *Setd4-CreER^{T2}::mTmG* mice were treated with TAM at P3, then analyzed at P4, P21, and P56 (Figure 1H). Almost all GFP$^+$ cells expressed markers of NSCs but lacked the cell proliferation marker of KI67, each maintained as a single-cell clone in the SVZ throughout all time points (Figures 1I, S2B, and S2C). These SETD4$^+$ NSCs still showed typical radial morphology along the SVZ at P56 (Figure 1I). Previous reports have shown that NBs derived from SVZ NSCs migrate to the OB and distribute to the granule cell layer (GCL) and the glomeruli (Lim and Alvarez-Buylla, 2016). Here, we did not observe any progeny (GFP$^+$) of SETD4$^+$ NSCs in the OB, indicating that these SETD4$^+$ NSCs were maintained in a quiescent state in the SVZ during postnatal development (Figures 1I and S2D). The long-term behavior of SETD4$^+$ quiescent NSCs was also examined by lineage tracing in adult (2-month-old) *Setd4-CreER^{T2}::mTmG* mice. After 1 and 12 months of TAM induction, GFP$^+$ cells were observed as remaining as single-cell clones in the wall

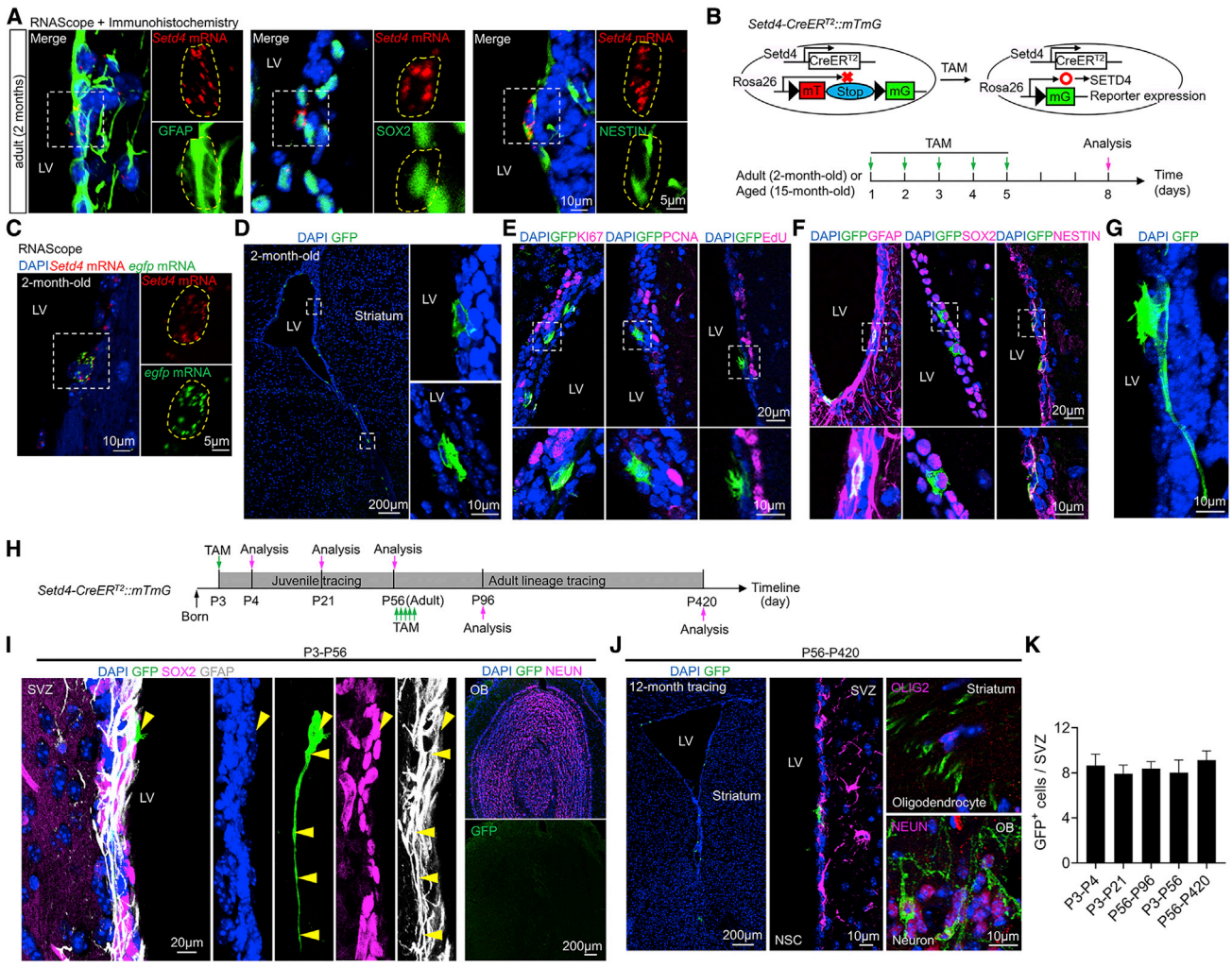

Figure 1. SETD4 marks long-lived quiescent NSCs in the SVZ of adult brain

(A) Confocal images of *in situ* hybridization of *Setd4* expression using RNAscope and combined with immunostaining for the NSC markers GFAP, SOX2, and NESTIN in the adult SVZ of C57BL/6 mice. The boxed area represents a higher magnification. The yellow dotted circle highlights a *Setd4*$^+$ cell.

(B) Schematic representation of *Setd4-CreER*^{T2} lineage tracing mice. Adult lineage tracing mice were injected with TAM and chased after 3 days for the following analyses.

(C) Confocal images of *in situ* hybridization of *Setd4* and *egfp* expression using RNAscope in the adult SVZ of *Setd4-CreER*^{T2}*::mTmG* mice after 3 days of TAM induction. A higher magnification is showed in the boxed area. The yellow dotted circle highlights a *Setd4*$^+$ cell.

(D) Confocal images of GFP$^+$ cells in the whole SVZ of 2-month-old mice with higher magnification boxed area (right).

(E and F) Confocal images of cell proliferation markers (KI67 and PCNA), EdU-incorporated signal (E) and the NSC markers GFAP, SOX2, and NESTIN (F) in GFP$^+$ cells in the SVZ (top) of 2-month-old mice. A higher magnification is showed in the boxed area (bottom).

(G) Representative image of a SETD4$^+$ cell in the SVZ of 2-month-old mice, with a representative minute apical ending to the ventricular surface and a long basal process.

(H) Experimental overview. Postnatal *Setd4-CreER*^{T2}*::mTmG* mice were injected with TAM at P3 for lineage-tracing analysis at P4, P21, and P56. Adult *Setd4-CreER*^{T2}*::mTmG* mice were injected with TAM at P56 for extended period lineage-tracing analyses at different time points.

(I) Confocal images of immunostaining for NSC markers in GFP$^+$ cells in the SVZ at P56 (left) and the mature neuron marker NEUN in the OB (right). The yellow arrowhead signifies a single NSC (GFP$^+$SOX2$^+$GFAP$^+$) and its radial process.

(J and K) Confocal images of GFP$^+$ cells consisting of a single NSC (GFAP$^+$) in the SVZ and few progenies including oligodendrocytes (OLIG2$^+$) in the striatum (top) and neurons (NEUN$^+$) in the OB (bottom) after 12 months of TAM induction (J). Quantification of the number of GFP$^+$ cells in lineage tracing experiments of adolescent and adult mice (K).

Nuclei were stained with DAPI (blue). LV, lateral ventricle; OB, the olfactory bulb. n = 4 mice were analyzed in each experiment.

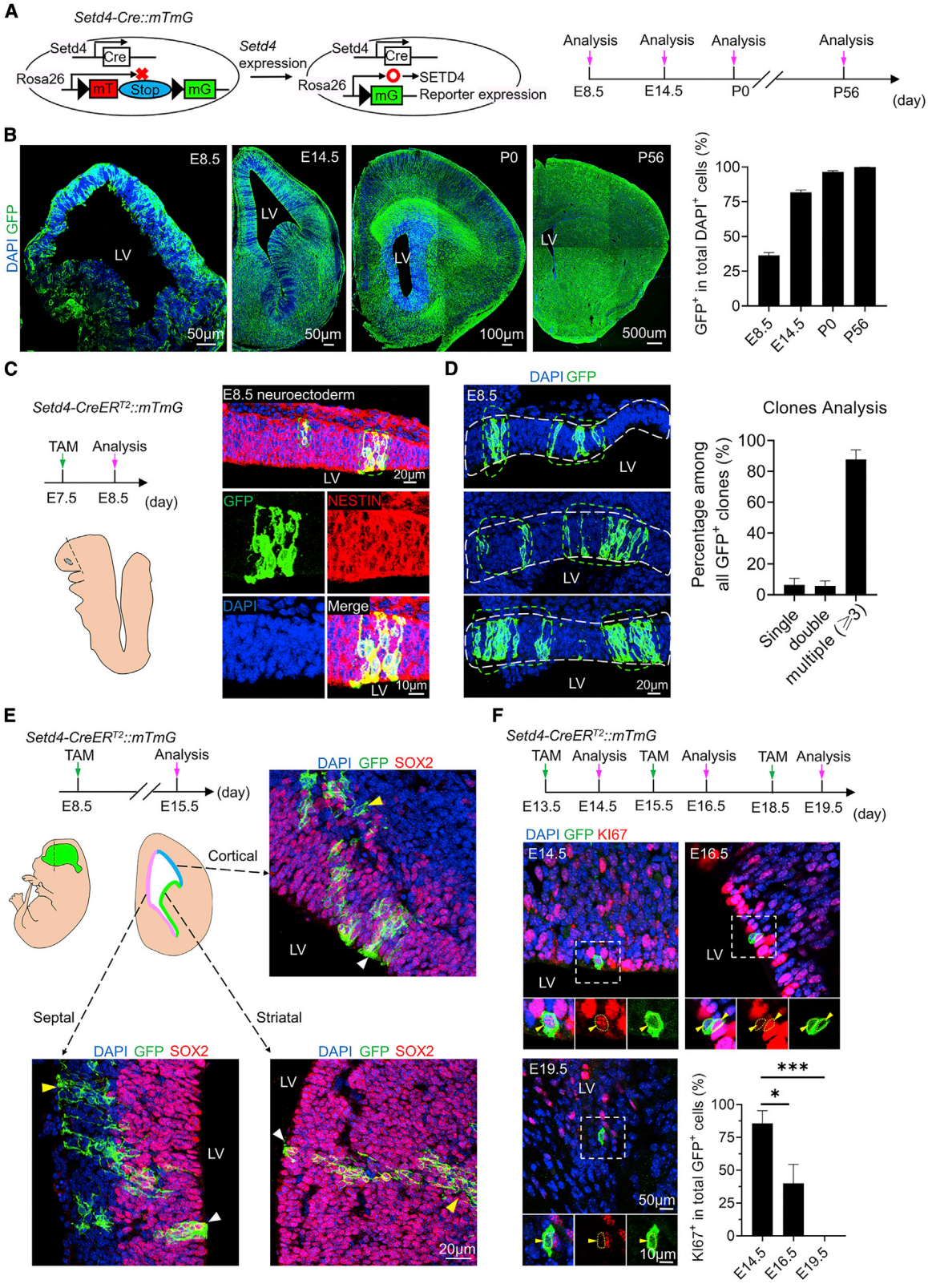

(legend on next page)

of the SVZ (Figures 1J and S2E). At very low cell numbers, GFP$^+$OLIG2$^+$ oligodendrocytes in the striatum and GFP$^+$NEUN$^+$ neurons in the GCL of the OB were identified, showing that SETD4$^+$ quiescent NSCs are long lived and have neurogenic capacity. We found that lineage tracing of adolescent and adult SETD4$^+$ NSCs resulted in ~8 GFP$^+$ cells per SVZ examined, and the number of GFP$^+$ cells did not change over time (Figure 1K). These results reveal that a small population of long-lived SETD4$^+$ quiescent NSCs occur from embryo to the adult SVZ.

Embryonic SETD4$^+$ cells contribute to brain development in the early embryo, then enter quiescence in the late embryo

As the earliest neural stem cells, radial glia cells (RGCs), derived from neuroepithelial cells (NECs), arise around embryonic day 10.5 (E10.5) (Kriegstein and Gotz, 2003; Kriegstein and Alvarezbuylla, 2009). They then contribute to both embryonic and postnatal neurogenesis, giving rise to all the neuronal and glial lineages of the CNS (Anthony et al., 2004; Merkle et al., 2004). However, the early embryonic origins of NECs remain unclear. Before embryonic neurogenesis, the neuroectoderm is composed of a single layer of NECs, which form between E6.5 and E10.5 (Gotz and Huttner, 2005). Considering that the CNS originates from this, we generated *Setd4-Cre::mTmG* mice, which permitted observation of the descendants of SETD4$^+$ cells without the requirement of TAM induction (Figure 2A). We performed identification of GFP$^+$ cells in the neuroepithelium at E8.5, the developing CNS at E14.5, and the neonatal brain at P0. We found that GFP$^+$ cells, including SETD4$^+$ and their daughter cells, constituted more than 36.40% ± 2.0% in the neuroectoderm at E8.5, which increased to more than 88.20% ± 4.83% and 96.40% ± 0.97% in the embryonic ventricular zone (VZ) at E14.5 and the SVZ at P0, respectively (Figure 2B). From E8.5 to P0, these GFP$^+$ cells were identified via detection of NESTIN and SOX2 to label the majority of NECs in the neuroectoderm, then RGCs in the embryonic VZ and NSCs in the SVZ (Figure S3A). TUJ1 detection confirmed that these GFP$^+$ cells also largely contributed to neurons (TUJ1$^+$) in the embryonic and neonatal brain (Figure S3A). Interestingly, beyond developmental stages, these GFP$^+$ cells were also identified as distributed throughout the entire brain of adult *Setd4-Cre::mTmG* mice at P56, including the OB, striatum, cortex, SVZ, and SGZ regions (Figure S3B). Colocalization analysis via cytoplasmic-localized reporter (*Setd4-Cre::Luc-EGFP*) further validated our observation that almost all cells were indeed GFP positive at P56, including the radial glial-like cells in SGZ (Figure S3C). Flow cytometric analysis showed that approximately 98.33% ± 0.24% cells were GFP positive of the whole brain (Figure S3D). These results suggest that fetal SETD4$^+$ cells occurring at very early embryonic stages were vital to the origin of subsequent brain development.

To further investigate fate specification of individual early embryonic SETD4$^+$ cells, we next administered TAM to pregnant female *Setd4-CreER^{T2}::mTmG* mice at E7.5 and chased at E8.5 before the neuroepithelium was fully specified in the embryos. The GFP$^+$ cells were identified in the neuroectoderm with NESTIN positive as NECs (Figure 2C). The GFP$^+$ clones consisted of single, double, or multiple cells, indicating that SETD4$^+$ cells had occurred at E7.5 and contributed to NEC population in the neuroepithelium (Figure 2D). To examine whether this GFP$^+$ population produces fetal RGCs and neurons during embryonic neurogenesis, we performed a single TAM pulse at E8.5 and chase at E15.5 (Figure 2E). As expected, these GFP$^+$ clones were observed in cortical, striatal, and septal sides of the VZ in the forebrain. Upon immunostaining with SOX2, these GFP$^+$ clones were further confirmed as consisting of RGCs (GFP$^+$SOX2$^+$), and their migrating differentiated progeny (GFP$^+$SOX2$^-$). These

Figure 2. Embryonic SETD4$^+$ cells contribute to brain development then enter quiescence in the late embryo

(A) Schematic representation of *Setd4-Cre* lineage tracing mice. Experimental overview. Analysis of embryonic and adult mouse brain from timed-pregnant *Setd4-Cre::mTmG* female mice at E8.5, E14.5, P0, or P56.

(B) Confocal images and quantification of GFP$^+$ cells in the neuroepithelium at E8.5 and the SVZ at E14.5, P0, and P56.

(C and D) Experimental overview. Timed-pregnant *Setd4-CreER^{T2}::mTmG* female mice received one injection of TAM at E7.5. Embryos were analyzed at E8.5. The dark dashed line indicates the position of the section. Confocal images of GFP$^+$ clones consisting of NECs in the neuroepithelium (top) with a higher magnification (bottom) (C). Representative images (left) of rare clones which co-existed in the neuroepithelium and quantification (right) of GFP active clone compositions (single, double, or multiple cells per clone) (D). The green dotted circle line highlights a clone.

(E) Timed-pregnant *Setd4-CreER^{T2}::mTmG* female mice received one injection of TAM at E8.5.Embryos were analyzed at E15.5. The dashed line indicates the position of the section. Confocal images of GFP$^+$ clones consisting of RGCs with radial morphology and SOX2$^+$ (white arrows) and their progeny cells (yellow arrows) in the cortical (blue), striatal (green), and septal (pink) SVZ of the forebrain.

(F) Timed-pregnant *Setd4-CreER^{T2}::mTmG* female mice received one injection of TAM at E13.5, E15.5, or E18.5, and embryos were analyzed 1 day after TAM induction. Confocal images of GFP$^+$ clones co-stained with KI67 (top) and with higher magnification boxed area (bottom). Quantification of the percentage KI67$^+$GFP$^+$ cells from animals injected at different time points.

Nuclei were stained with DAPI (blue). LV, lateral ventricle. Values represent mean ± SEM. n > 3 embryos or mice were analyzed in (A), (C), (E), and (F). n = 83 clones analyzed in (D). n > 12 clones were analyzed at each time point in (F). *p < 0.05 and ***p < 0.001.

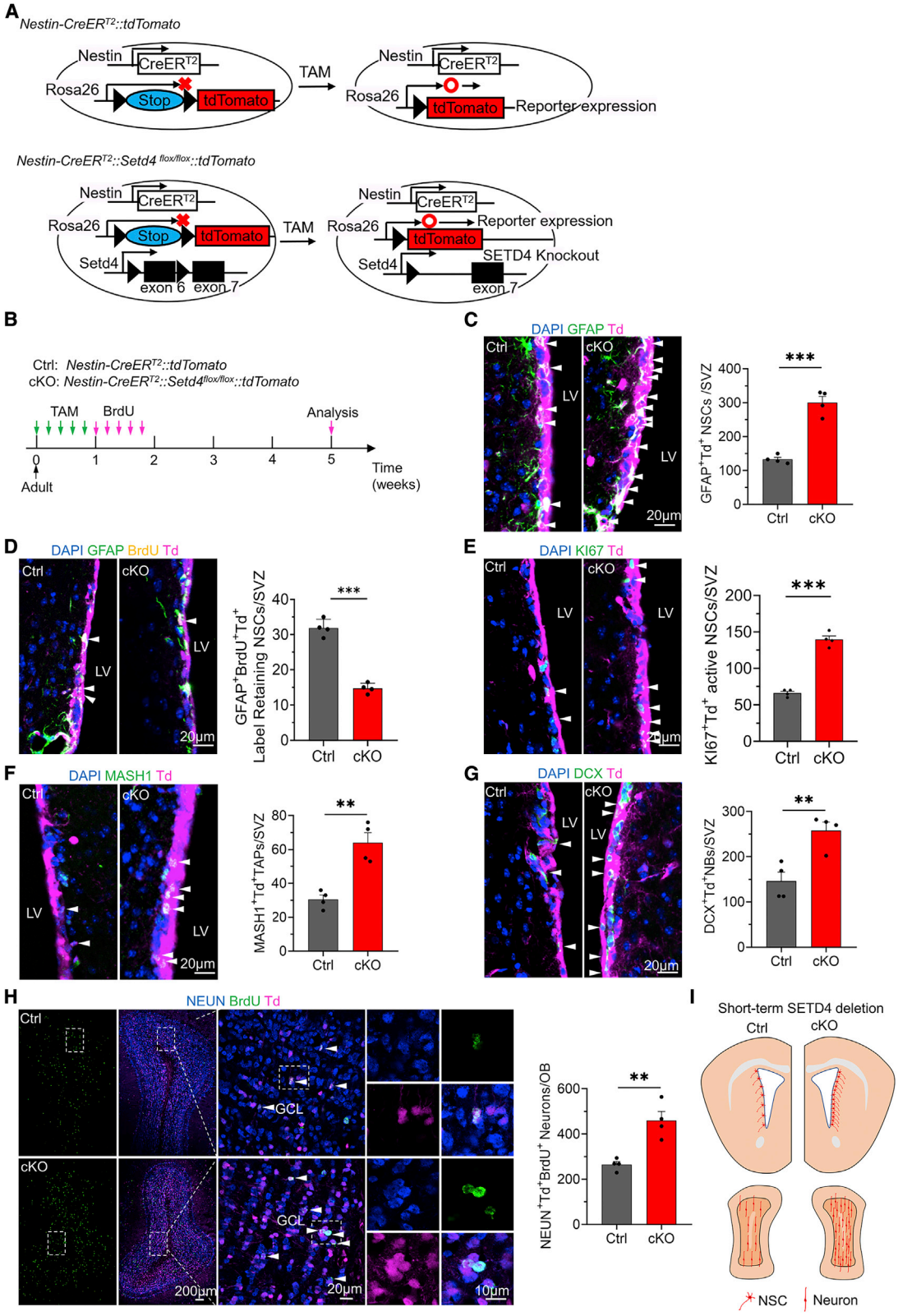

(legend on next page)

results demonstrate that SETD4$^+$ cells originate NECs, then generate RGCs that contribute to embryonic neurogenesis in the forebrain.

Previous research has demonstrated that RGCs can enter a quiescent state between E13.5 and E15.5, which can then persist for a long period into the adult SVZ (Fuentealba et al., 2015; Furutachi et al., 2015). To directly assess whether SETD4$^+$ cells enter a quiescent state during embryonic development, we injected pregnant female *Setd4-CreER^{T2}::mTmG* mice with TAM at E13.5, E15.5, and E18.5 (Figure 2F). One day later, embryos were examined for the presence of GFP$^+$ cells. The GFP$^+$ cells showed the characteristic morphology of RGCs with long radial fibers on the ventricular surface at all time points. We examined the division state of these cells by immunostaining for KI67. The percentages of KI67$^+$GFP$^+$ cells decreased from 85.71% ± 9.71% at E14.5 to 40.00% ± 14.53% at E16.5 and then dropped to zero at E19.5, indicating SETD4$^+$ cells had entered a quiescent state during that period. These results show that SETD4$^+$ cells appear in the early embryo, contribute to brain development, and then enter quiescence before birth.

Conditional knockout of *Setd4* activates quiescent NSCs and rapidly promotes neurogenesis

The functions of these long-lived quiescent NSCs could be examined only after their activation. Because of the NSC marker's expression in SETD4$^+$ cells, *Setd4* conditional knockout (cKO) was constructed by generating *Nestin-CreER^{T2}::Setd4$^{flox/flox}$::tdTomato* (SETD4 cKO) mice (Figure 3A). To activate SETD4$^+$ quiescent NSCs, we performed *Setd4* cKO in adult SETD4 cKO mice (Figure S4A). Adult *Nestin-CreER^{T2}::tdTomato* reporter mice were used as a control, and the majority of the NESTIN$^+$ NSCs were labeled with tdTomato (Td). After 3 days of TAM induction, the expression of SETD4 in the SVZ had been abolished, as indicated by western blot analysis, showing that SETD4 cKO mice had been successfully constructed (Figure S4A). Meanwhile, we observed a significant increase of active NSCs (KI67$^+$Td$^+$) in contrast to controls (Figure S4B). This indicated that deletion of SETD4 had resulted in the activation of quiescent NSCs, enabling entrance into the cell cycle. This progress was also supported by a significant increase of EdU-labeled NSCs (EdU$^+$Td$^+$) after 2 h of EdU incorporation in SETD4 cKO mice (Figure S4C). At 3 days, the increased proliferation of NSCs had not affected the number of Td$^+$GFAP$^+$ NSCs in the SVZ of the SETD4 cKO mice (Figure S4D). This suggested that deletion of SETD4 causes activation of SETD4$^+$ quiescent NSCs.

Next, we extended the study to one month to identify the effect of SETD4 deletion on NSC activation and the differentiation of their progeny (Figure 3B). One month after deletion, the number of GFAP$^+$Td$^+$ NSCs had significantly increased in the SVZ of SETD4 cKO mice compared with control mice (Figure 3C), in which the numbers of BrdU label-retaining NSCs (GFAP$^+$BrdU$^+$Td$^+$) and active NSCs (KI67$^+$Td$^+$) decreased and increased, respectively (Figures 3D and 3E). SETD4 deletion also led to significant increases of newborn TAPs (MASH1$^+$Td$^+$) and NBs (DCX$^+$Td$^+$) in the SVZ and progeny neurons (NEUN$^+$Td$^+$) in the OB (Figures 3F–3H). These demonstrated a strengthening of neurogenesis of SETD4 cKO mice. We propose that one month of SETD4 deletion was sufficient to both activate the quiescent NSCs in the SVZ and then give rise to newborn neurons in the OB.

To validate this, we also performed *Setd4* cKO in the SVZ of adult *Setd4$^{flox/flox}$::tdTomato* mice by injection of AAV9-GFAP-Cre (Figure S4E). As observed in the SETD4 cKO mice after one month of TAM induction, the number of SOX2$^+$Td$^+$ NSCs had significantly increased after 6 weeks of SETD4 deletion, in contrast to controls (Figure S4F). Correspondingly, the numbers of active NSCs (KI67$^+$Td$^+$), TAPs (MASH1$^+$Td$^+$), and NBs (DCX$^+$Td$^+$) in the SVZ and their progeny neurons (NEUN$^+$Td$^+$) in the GCL of the OB had also increased after SETD4 deletion (Figures S4G–S4J). These findings show that the deletion of SETD4 causes quiescence exit of quiescent NSCs and increased neurogenesis, resulting in more newborn neurons in the OB and strengthening the suggestion that SETD4 regulates the maintenance of quiescence of NSCs (Figure 3I).

Persistent knockout of *Setd4* results in NSC exhaustion and a decrease in neurogenesis

Age-related decline in adult neurogenesis has been linked to NSC exhaustion (Signer and Morrison, 2013; Shi et al., 2018). Although over a shorter period of one month, we

Figure 3. Conditional knockout of *Setd4* rapidly promotes neurogenesis

(A) Schematic representation of *Nestin-CreER^{T2}::tdTomato* control mice and *Nestin-CreER^{T2}::Setd4$^{flox/flox}$::tdTomato* mice.

(B) Experimental overview. Control and *Setd4* cKO mice were pulsed with TAM injection, followed by BrdU injection and analyses in (C)–(H) after one month of TAM induction.

(C–H) Confocal images and quantification of total NSCs (GFAP$^+$Td$^+$) (C), BrdU label-retaining NSCs (GFAP$^+$BrdU$^+$Td$^+$) (D), active NSCs (KI67$^+$Td$^+$) (E), TAPs (MASH1$^+$Td$^+$) (F), NBs (DCX$^+$Td$^+$) (G) in the SVZ of lateral ventricles, and newborn neurons (NEUN$^+$BrdU$^+$Td$^+$) (H) in the GCL of OB in control (Ctrl) or *Setd4* cKO mice.

(I) Summary of the effects of one month *Setd4* cKO mice on NSCs in the SVZ and newborn neurons in the OB.

Nuclei were stained with DAPI (blue). GCL, granule cell layer; OB, olfactory bulb. Values represent mean ± SEM. **p < 0.01 and ***p < 0.001. n = 4 mice.

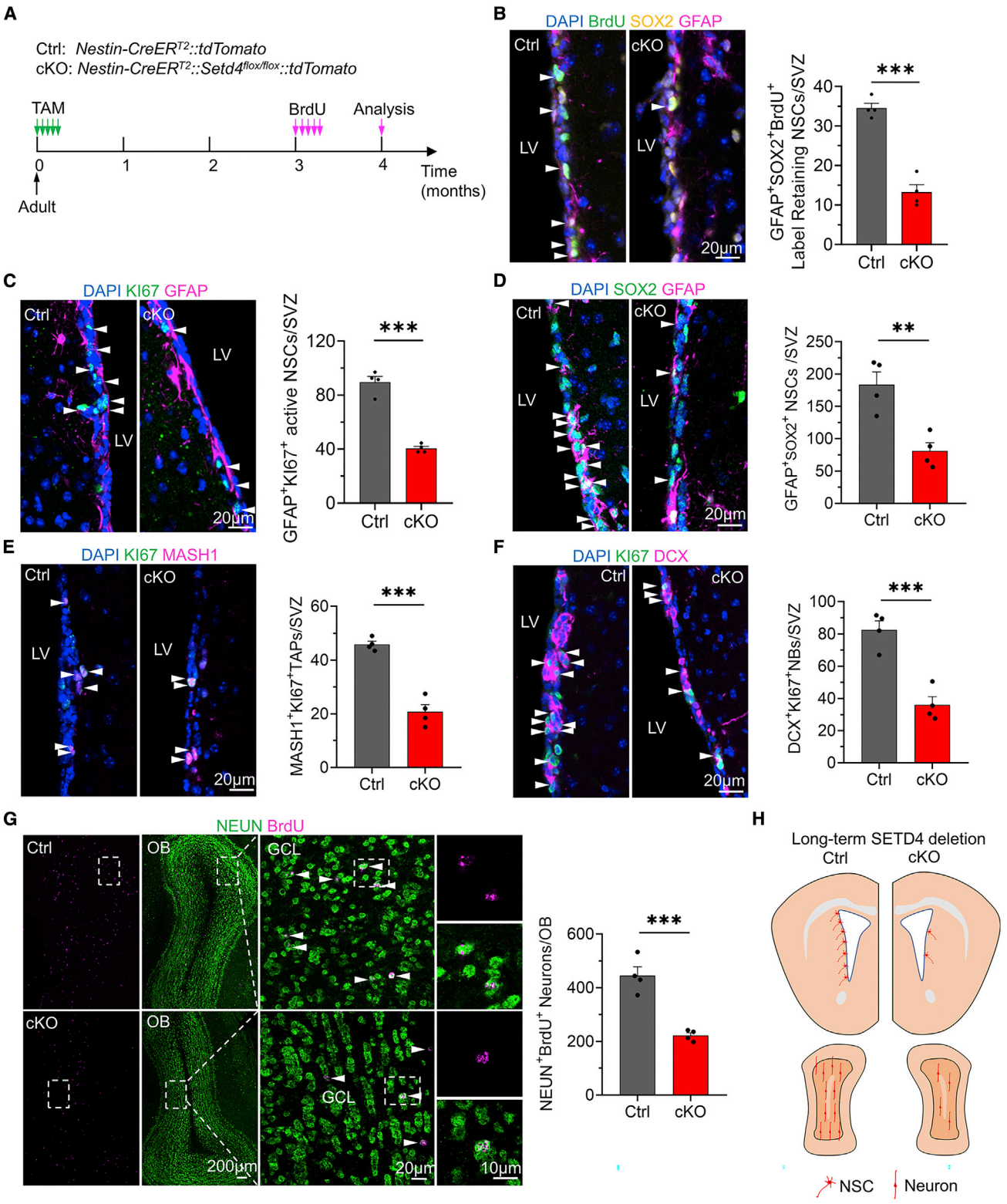

Figure 4. Long-term deletion of SETD4 results in NSC exhaustion and decrease of neurogenesis

(A) Experimental overview. Control and *Setd4* cKO mice were pulsed with TAM injection, followed by BrdU injection after 3 months of TAM induction and analyses in (B)–(G) after 4 months of TAM induction.

(legend continued on next page)

had observed that *Setd4* cKO causes an increase in neurogenesis, we then examined the longer term consequences of SETD4 deletion. We extended TAM induction to 4 months in adult SETD4 cKO mice and labeled NSCs in the SVZ and newly generated neurons in the OB (Figure 4A). BrdU label-retaining NSCs, $GFAP^+SOX2^+BrdU^+$ cells had significantly reduced in the SVZ after 4 months *Setd4* cKO (Figure 4B). This was in line with the observation that the numbers of active NSCs ($GFAP^+KI67^+$) and $GFAP^+SOX2^+$ NSCs had also decreased (Figures 4C and 4D). Long-term *Setd4* cKO in mice also showed a significant reduction in TAPs ($MASH1^+KI67^+$) and NBs (DCX^+KI67^+) and BrdU label-retained newborn neurons ($NEUN^+BrdU^+$) in the GCL of the OB, compared with those of controls (Figures 4E–4G). We concluded that persistent deletion of SETD4 leads to depletion of the NSC reservoir and removal of their corresponding neurogenic abilities (Figure 4H).

In addition, we specifically knocked out *Setd4* using a *UBC-CreER^{T2}* driver (Figure S5A). We observed that ablation of SETD4 in *UBC-CreER^{T2}::Setd4$^{flox/flox}$* mice led to similar results to those of long-term *Setd4* cKO in SETD4 cKO mice with the overall number of $GFAP^+SOX2^+$ NSCs, BrdU label-retaining NSCs active NSCs, TAPs and NBs in the SVZ, and newborn neurons in the GCL of the OB all being decreased in contrast to the controls (Figures S5B–S5G). In conclusion, SETD4 may function to sustain quiescent NSCs, thus protecting NSCs from exhaustion and retaining their neurogenesis potential in the adult.

Beyond activation, SETD4$^+$ quiescent NSCs promote regeneration in the injured OB

To investigate whether, beyond their activation, $SETD4^+$ quiescent NSCs are the instigators of regeneration, we injured right side of the OB of adult SETD4 cKO mice by N-methyl-D-aspartic acid (NMDA) injection, leaving the left side undamaged as a control. Examinations then begun after one month of *Setd4* cKO by TAM induction (Figure 5A). Following one week BrdU label-retaining and 3 week chase, BrdU signals were used to mark newborn neurons after NMDA induced injury. We found that the size of the injured OB recovered to the control levels after one month of injury (Figure 5B). As newborn neurons, the number of $BrdU^+Td^+$ cells significantly increased in the injured OB (Figure 5C). Moreover, along with the regeneration after *Setd4* cKO, active NSCs ($Td^+GFAP^+KI67^+$) markedly increased in the SVZ, an observation that may support neurogenesis of the injured OB (Figure 5C).

To assess such a contribution to neurogenesis in the injured OB by the activation of quiescent NSCs after *Setd4* cKO, we also performed the OB injury in adult *Nestin-CreER^{T2}::tdTomato* control mice without *Setd4* cKO (Figure S6A). Although newborn neurons labeled by BrdU increased in the injured OB compared with control OB (Figure S6B), the level of newborn neuron numbers in control mice (without *Setd4* cKO) was significantly lower than that in SETD4 cKO mice after one month of *Setd4* cKO (Figure S6C). Notably, no discernible change in active NSCs ($KI67^+GFAP^+Td^+$) was observed in the SVZ in control mice after one month OB injury (Figure S6D). These results indicate that, one month beyond activation of *Setd4* cKO, these quiescent NSCs were enabled to promote the regeneration of the injured OB.

However, if *Setd4* cKO occurred a considerable period before OB injury, the previous positive effects were reversed. If OB injury was induced after a delay of 4 months beyond *Setd4* cKO in SETD4 cKO mice, after a further 1 month, the size of the OB injured side showed a significant decrease in size and an atrophic appearance, in contrast to the left side control (Figure 5E). The number of newborn neurons ($BrdU^+Td^+$) in the OB labeled by BrdU and active NSCs ($GFAP^+KI67^+Td^+$) in the SVZ showed no further changes between injured-side OB and control-side OB, indicating that the regenerative capacity for injury repair had been compromised (Figures 5F and 5G). We propose that $SETD4^+$ quiescent NSCs are critical to protect the NSCs from exhaustion and to retain neurogenesis capacity in the adult, in which SETD4 may also be active a maintaining a stable quiescent NSCs number in the SVZ throughout the lifetime.

Overexpression of *Setd4* results in NSC quiescence entry and suppresses neurogenesis

In contrast to the consequences of SETD4 deletion, we also performed overexpression (OE) of *Setd4* in NSCs via generating *Nestin-CreER^{T2}::Rosa26-Setd4::tdTomato* (SETD4 OE) mice (Figure 6A). Upon RNAscope analysis, we observed that more SVZ NSCs expressing *Setd4* mRNA after 3 days of TAM induction compared with controls (Figures S7A and S7B). The expression level of SETD4 protein in the SVZ had also been up-regulated successfully (Figure S7C). This overexpression of SETD4 resulted in a significant

(B–G) Confocal images and quantification of BrdU label-retaining NSCs ($BrdU^+SOX2^+GFAP^+$) (B), active NSCs ($KI67^+GFAP^+$) (C), total NSCs ($SOX2^+GFAP^+$) (D), TAPs ($KI67^+MASH1^+$) (E), NBs ($KI67^+DCX^+$) (F) in the SVZ, and newborn neurons ($NEUN^+BrdU^+$) (G) in the GCL of the OB in control (Ctrl) and *Setd4* cKO mice.

(H) Summary of the effects of 4 month *Setd4* cKO mice on NSCs in the SVZ and production of newborn neurons in the OB.

Nuclei were stained with DAPI (blue). GCL, granule cell layer; OB, olfactory bulb. Values represent the mean ± SEM. $^{**}p < 0.01$ and $^{***}p < 0.001$. n = 4 mice.

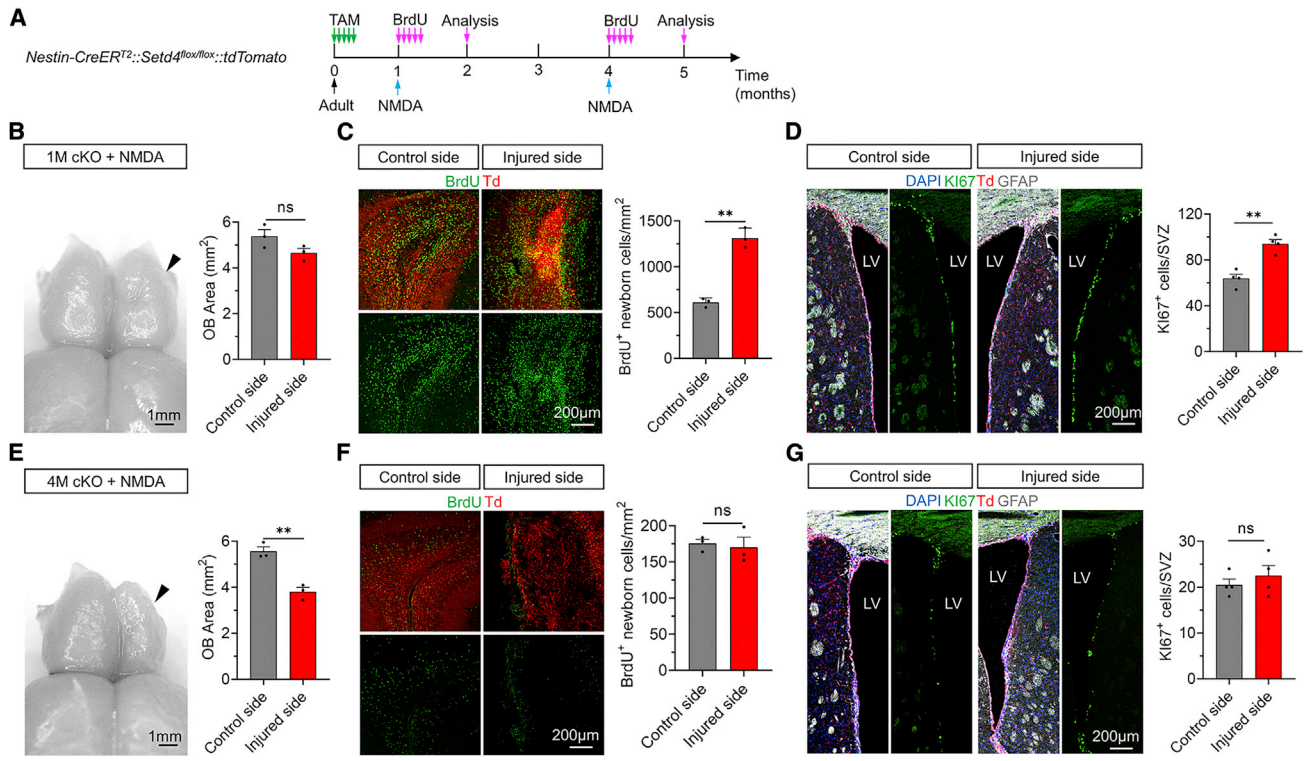

Figure 5. Beyond activation, SETD4$^+$ NSCs promote regeneration and repair in the injured OB

(A) Experimental overview. Control and *Setd4* cKO mice were pulsed with TAM injection, followed by NMDA injury and BrdU injection and analyses after 2 months of TAM induction in (B)–(D) and 5 months of TAM induction in (E)–(G).

(B) Picture and size of the OB in *Setd4* cKO mice. Right-side OBs (black arrow) were injured by NMDA, and left sides were left intact as a control. Pictures taken after 2 months of TAM induction.

(C and D) Confocal images and quantification of newborn cells (BrdU$^+$) in the GCL (C) and active NSCs (GFAP$^+$KI67$^+$Td$^+$) in the SVZ (D) in control side and injured side of *Setd4* cKO mice after 2 months of TAM induction.

(E) Picture and size of OB in *Setd4* cKO mice. Right-side OBs (black arrow) were injured by NMDA, and left sides were left intact as a control. Pictures taken after 5 months of TAM induction.

(F and G) Confocal images and quantification of newborn cells (BrdU$^+$) in the GCL (F) and active NSCs (GFAP$^+$KI67$^+$Td$^+$) in the SVZ (G) in control side and injured side of *Setd4* cKO mice after 5 months of TAM induction.

Nuclei were stained with DAPI (blue). LV, lateral ventricle; OB, olfactory bulb. Values represent mean ± SEM. **p < 0.01. n = 4 mice.

decrease in the number of active NSCs, as confirmed by detection of KI67 and assay of EdU incorporation (Figures S7D and S7E), indicating that the self-renew ability of NSCs has been abolished. The overall number of GFAP$^+$Td$^+$ NSCs in the SVZ remained unchanged compared with those in control mice (Figure S7F). These data suggested that SETD4 conveys quiescence to SVZ NSCs.

We then investigated the effects of *Setd4* OE after one month (Figure 6B). We observed that the number of Td$^+$GFAP$^+$ NSCs in the SVZ of one month SETD4 OE mice were significantly fewer than those in the control mice in normal physiological conditions, as the inhibition of NSC self-renews (Figure 6C). Meanwhile, the numbers of active NSCs (Td$^+$KI67$^+$) were also decreased beyond *Setd4* OE (Figure 6D). It is tempting to speculate that the normal neurogenesis progress was suppressed. In line with this, the numbers of TAPs (Td$^+$MASH1$^+$) and NBs (Td$^+$DCX$^+$) in the SVZ were reduced (Figures 6E and 6F). Importantly, the significant decrease of newborn neurons (NEUN$^+$BrdU$^+$) in the GCL of the OB, and the link of this to the global decrease in these cells, indicated that overexpression of *Setd4* induces NSCs to enter a quiescent state, leading to deprivation of their subsequent neurogenic capabilities (Figures 6G and 6H).

SETD4 epigenetically regulates the quiescence of NSCs via multiple signaling pathways

To investigate whether SETD4 epigenetically controls NSC quiescence via the previously noted conserved mechanism by which heterochromatin formation was facilitated via H4K20ME3 catalysis (Dai et al., 2017; Ye et al., 2019), we performed immunostaining for H3K9AC (a marker of

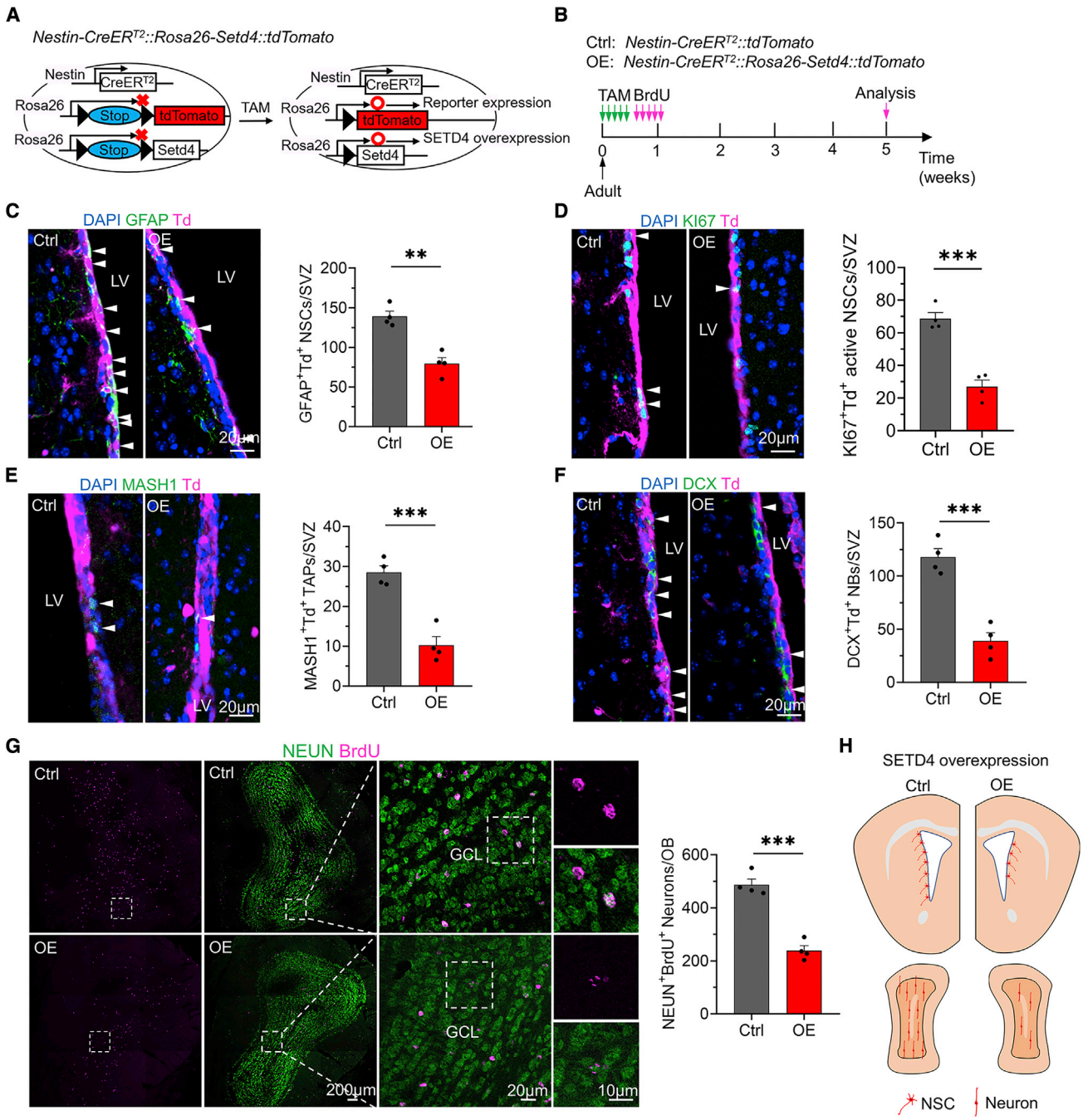

Figure 6. Overexpression of *Setd4* results in quiescence entry of NSCs and a decrease of neurogenesis

(A) Schematic representation of *Nestin-CreER^{T2}::Setd4::tdTomato* mice.

(B) Experimental overview. Control (Ctrl) and *Setd4* overexpression (OE) mice were pulsed with TAM injection, followed by BrdU injection and analyses in (C)–(G) after one month of TAM induction.

(C–G) Confocal images and quantification of total NSCs (GFAP$^+$Td$^+$) (C), active NSCs (KI67$^+$Td$^+$) (D), TAPs (MASH1$^+$Td$^+$) (E), NBs (DCX$^+$Td$^+$) (F) in the SVZ of lateral ventricles, and newborn neurons (NEUN$^+$BrdU$^+$) (G) in the GCL of the OB in control and *Setd4* overexpression mice.

(H) Summary of the effects of one month *Setd4* overexpression mice on NSCs in the SVZ and the production of newborn neurons in the OB. Nuclei were stained with DAPI (blue). GCL, granule cell layer; OB, olfactory bulb. Values represent the mean ± SEM. **p < 0.01 and ***p < 0.001. n = 4 mice.

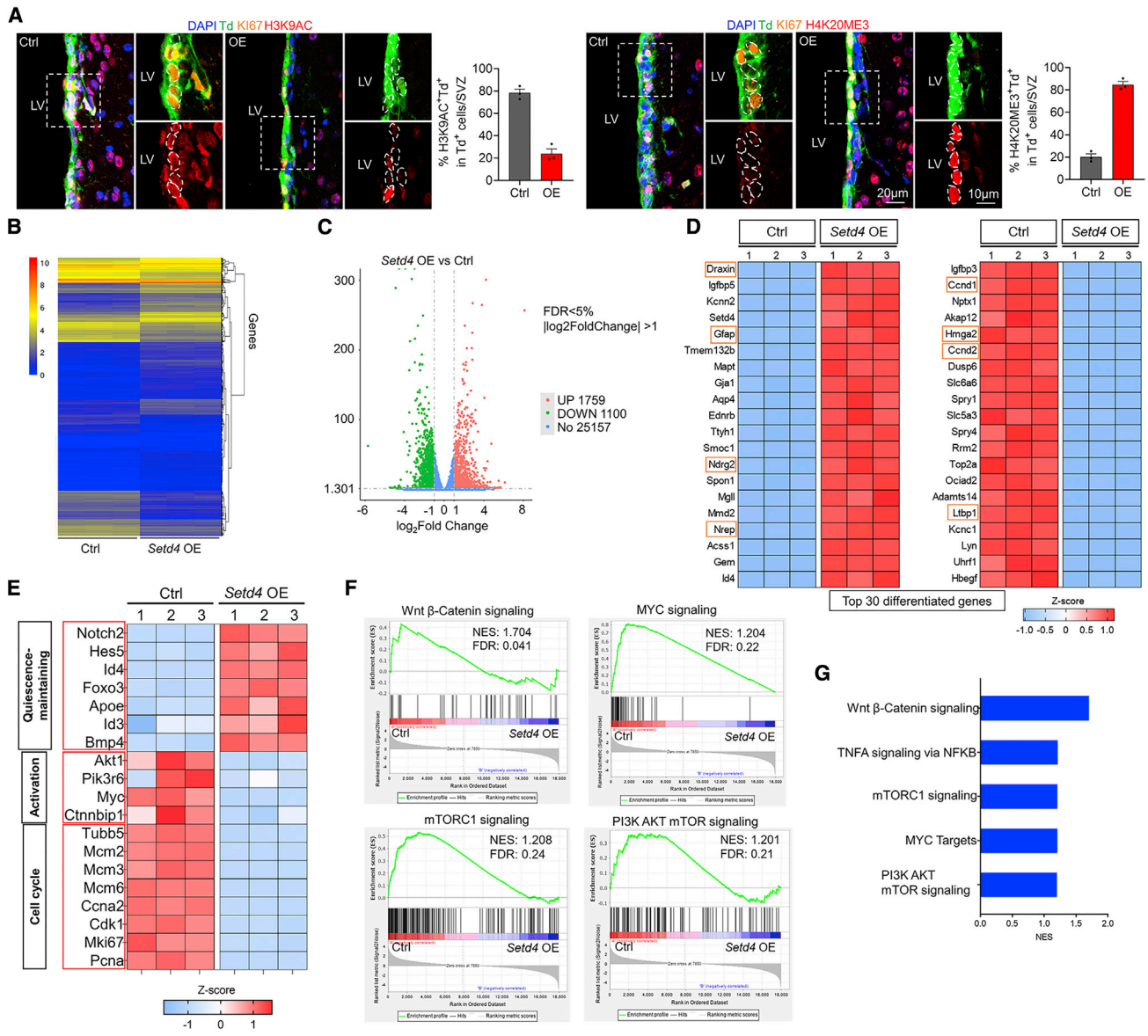

Figure 7. SETD4 epigenetically regulates quiescence of NSCs via multiple signaling pathways

(A) Confocal images and quantification of the level of H3K9AC and H4K20ME3 in NSCs in the SVZ of lateral ventricles in control and *Setd4* overexpression mice after 3 day TAM induction. The white dotted circle line highlights the nuclear location of the higher magnification boxed area.

(B) Heatmap of gene expression in primary adult SVZ NSCs after *Setd4* overexpression using RNA-seq.

(C) Volcano plot of total changed genes after *Setd4* overexpression.

(D and E) Heatmap of differentially expressed genes from top 30-folded-changed genes (D) and representative gene expression for NSC quiescence-maintaining, activation, and cell cycle (E) after *Setd4* overexpression.

(F and G) Gene set enrichment analysis (GSEA) (F) and Kyoto Encyclopedia of Genes and Genomes (KEGG) pathway enrichment analysis (G) after *Setd4* overexpression.

Nuclei were stained with DAPI (blue). LV, lateral ventricle. Data are represented as mean ± SEM. n = 3 mice were analyzed per experiment. Student's t test.

euchromatin) and H4K20ME3 (a marker of heterochromatin) to analyze the changes in the epigenetic state of adult NSCs after *Setd4* OE. We observed that SETD4 overexpression induced an increase of H4K20ME3 and decrease of H3K9AC in NSCs (Td^+), in direct contrast to the situation of active NSCs (Td^+KI67^+) (Figure 7A). This was also

consistent with our observation of high H4K20ME3 levels and low H3K9AC levels in SETD4$^+$ (GFP$^+$) cells dissociated from SVZ of *Setd4-CreER^{T2}::mTmG* (Figure S7G).

Next, we aimed to reveal molecular mechanisms by which SETD4 controls the quiescence of NSCs in the adult SVZ. For this we performed RNA sequencing (RNA-seq) analysis in primary SVZ NSCs isolated from adult C57BL/6 mice that had been treated with either ADV-GFP (control) or ADV-SETD4-GFP (overexpression). Compared with the controls, 1,759 genes were found to be significantly up-regulated and 1,100 genes were down-regulated after *Setd4* overexpression, with a false discovery rate (FDR) $\leq$ 5% and $|\log_2(\text{fold change})| > 1$ (Figures 7B and 7C). Analysis of the differentially expressed genes showed that *Setd4* overexpression had resulted in significantly up-regulated expressions of quiescence-maintaining related genes including *Draxin*, *Ndrg2*, *Notch2*, *Id4*, *Foxo3*, *Apoe*, and *Bmp4* and down-regulated expressions of both activation-associated genes *Akt1*, *Pi3kr6*, *Myc*, *Ctnnbip1* and cell cycle genes, such as *Ccnd1*, *Ccnd2*, *Mcm2*, *Cdk1*, *Mki67*, and *Pcna* (Figures 7D and 7E). Gene set enrichment analysis and Kyoto Encyclopedia of Genes and Genomes orthology indicated that the NSC activation-associated signaling pathways of Wnt β-catenin, mTOR, PI3K-AKT, and MYC targets were all inhibited (Figures 7F and 7G). We conclude that SETD4 epigenetically controls quiescence of NSCs for sustaining a protected NSC population and maintaining a stem cell reservoir.

DISCUSSION

NSC quiescence does not simply occur in a uniform manner but is found to be heterogeneous. This diversity has been attributed to cells being at different depths of quiescence, forming a continuum of developmental stages along the quiescence to activity trajectory (Llorens-Bobadilla et al., 2015). Overall, it has been difficult to define NSCs in their quiescent state because of a lack of their specific markers. Identification of their exact function via tracing their lineages during brain homeostasis, damage repair and aging has likewise proved elusive. In this study, we found that SETD4$^+$ NSCs enter quiescence before birth and persist into the SVZ even through to 15-month-old mice, indicating that they remain in a deeply quiescent state over an extended period. SETD4 was then successfully used to mark a long-lived and deeply quiescent NSC population in the SVZ of adult mice. Long-term lineage tracing over one year showed that SETD4$^+$ NSCs maintain their quiescent state with a little or no progeny production in such a state of homeostasis. However, after one month activation by *Setd4* knockout, formerly quiescent NSCs showed increased numbers in the SVZ, also with the production of large number of newborn neurons in the OB. This neurogenesis significantly contributed to repair of the damaged OB. We suggest that the quiescence of SETD4$^+$ NSCs relating to brain injury or age-related senescence occurs firstly to protect the NSC reservoir from depletion and then to facilitate subsequent activation from quiescence for reparative and regenerative neurogenesis.

Results of *Setd4* cKO and overexpression indicate that, as a determinative factor, SETD4 modulates the quiescence of NSCs. We suggest that SETD4 epigenetically controls NSC quiescence via the previously noted conserved mechanism by which heterochromatin formation is facilitated via H4K20ME3 catalysis. As noted in our previous report (Ye et al., 2019), SETD4 may regulate genome-wide transcription effecting many downstream signaling pathways with a conserved mechanism. In the present study, though deletion of SETD4 resulted in quiescence exit of NSCs in the SVZ and promoted neurogenesis in the OB during an initial period, persistent deletion leaded to NSC exhaustion and subsequent decrease of neurogenesis. We propose that SETD4 may also endow quiescent NSCs with the potential for asymmetric division for maintenance of a consistent cell number in the SVZ throughout the lifetime.

Previous studies have manipulated the general neural cell precursors of various embryonic stages to examine the impact on the adult SVZ neural progenitor pool (Hu et al., 2017; Furutachi et al., 2015; Ohtsuka and Kageyama, 2021). During brain development, NSCs have been noted as contained within the lineages stemming from NECs in the fetal neuroepithelium to postnatal/adult B1 cells via RGCs (Kriegstein and Gotz, 2003; Kriegstein and Alvarez-buylla, 2009). Here, using *Setd4-Cre* and *Setd4-CreER^{T2}* mouse lines, we found that SETD4$^+$ cells appear before neuroectoderm formation, a very early stage of embryonic neurogenesis and generate NECs, the precursors of the earliest embryonic neural stem cells, RGCs. Combined with their capacities for contribution to almost the entire brain in adult *Setd4-Cre* mice, we suggest that these SETD4$^+$ cells originate the brain by generating a precursor population that includes both NECs and RGCs, which then contributes to all lineages of neurons during embryonic development. We also found that SETD4$^+$ cells in early embryos produced almost all postnatal NSCs both in the SVZ and SGZ (Figure S3D). However, we did not observe quiescent SETD4$^+$ NSCs in the adult SGZ, suggesting other distinct mechanisms for NSCs reservoir maintenance likely occur in the SGZ.

This appearance at a very early embryonic stage may endow SETD4$^+$ quiescent NSCs with high pluripotency or strong neurogenic capabilities. However, such pluripotency seems to be negated by *Setd4* knockout, which led to depletion of the NSC reservoir and removal of neurogenic capabilities over an extended period. We thus

conclude that SETD4 controls NSC quiescence to preserve a stem cell reservoir for retaining the function of neurogenesis over extended periods and contributes to regeneration after injury. Our findings provide SETD4 as a primary regulator, active in the switch between quiescence entrance and exit for NSCs, that governs the rate of neurogenesis in homeostasis and in response to damage. Moreover, our study may pave the way for future pharmacologic developments aimed at targeting quiescent NSCs with SETD4, potentially applicable to many aspects of brain damage and neurodegenerative disease.

EXPERIMENTAL PROCEDURES

Animals

All animal procedures used in this study were performed following the animal care guidelines approved by the Institutional Animal Care and Use Committee of Zhejiang University. The transgenic animals constructed and used in this study are shown in the supplemental methods. All transgenic mice in this study were backcrossed for at least five generations and maintained on a C57BL/6 background.

TAM treatment and administration of EdU or BrdU

A TAM solution (20 mg/mL) was prepared for intraperitoneal injections by dissolving the powder (#T5648; Sigma-Aldrich) in a 9:1 solution of corn oil/ethanol at 37°C with occasional vertexing until dissolved. The labeling of cells progressing though to S phase was performed by intraperitoneal injections of EdU (50 mg/kg; #E10187; Invitrogen), and animals were analyzed 2 h later. For the BrdU label-retaining test, BrdU was administrated in drinking water (1 mg/mL in 0.1% sucrose; #B5002; Sigma-Aldrich) for 1 week followed by a 3 week "chase" period.

Clonal analysis

For labeling of SETD4$^+$ cell clonal lineage analysis in embryos, the timed pregnancy was determined by identifying a vaginal plug (E0.5), and then a single dose of 80 mg/kg TAM was administered intraperitoneally to the pregnant females at the target embryonic day. A clone could be defined as a cluster of GFP$^+$ cells located along the neuroepithelium at E8.5 with a cell-to-cell distance of <100 μm. For labeling of SETD4$^+$ cells lineage tracing in neonates, mice were injected with a single dose of 80 mg/kg of TAM at P3. For population fate mapping of SETD4$^+$ cells in the adults and for the *Setd4* conditional knockout or overexpression study, a single dose of 160 mg/kg of TAM was intraperitoneally injected into mice every 24 h and repeated 5 times.

Immunofluorescent staining

The immunofluorescent staining details and antibodies used in this study are shown in the supplemental methods.

RNA sequencing

Total RNA for RNA-seq was extracted from primary NSCs using TRIzol reagent (#15596018; Invitrogen) after 24 h infection with ADV-GFP (Ctrl) and ADV-SETD4-GFP (*Setd4* OE), respectively. RNA-seq was performed at Tianjin Novogene Bioinformatics Technology Co., Ltd., using an Illumina HiSeq 4000 machine (see supplemental methods).

Statistical analysis

The studies were blinded during data collection and quantification. The data in figures reflect several independent experiments performed on different days. No data were excluded. Statistical analysis was performed with two-tailed unpaired Student's t tests, as indicated in the text and figures. All statistical analyses were performed in GraphPad Prism 8.0 software. All data are presented as mean ± SEM. A p value of <0.05 was considered to indicate statistical significance ($p > 0.05$ was considered to indicate not significant [NS]), with the exact p values stated in the corresponding figures.

Data and code availability

The processed bulk RNA sequencing data were deposited in the National Center for Biotechnology Information (NCBI) Gene Expression Omnibus (GEO) database under accession code GEO: GSE200159.

SUPPLEMENTAL INFORMATION

Supplemental information can be found online at https://doi.org/10.1016/j.stemcr.2022.07.017.

AUTHOR CONTRIBUTIONS

W.-J.Y. and S.-L.C. developed the concept and designed the study. S.-L.C. performed most of the research. W.-J.Y. supervised the research. W.-J.Y., S.-L.C., and Y.-S.Y. wrote the manuscript. Y.-S.Y., Y.-F.D., S.-H.Y., X.-Z.J., Y.-W.G., X.-T.H., and J.-S.Y., provided help in investigation and data analysis. C.W. provided advice during writing and proofread and revised the final manuscript.

ACKNOWLEDGMENTS

This work was supported by National Natural Science Foundation of China grant 31730084.

CONFLICTS OF INTEREST

The authors declare no competing interests.

Received: December 9, 2021
Revised: July 27, 2022
Accepted: July 27, 2022
Published: August 25, 2022

REFERENCES

Ahn, S., and Joyner, A.L. (2005). In vivo analysis of quiescent adult neural stem cells responding to Sonic hedgehog. Nature *437*, 894–897.

Anthony, T.E., Klein, C., Fishell, G., and Heintz, N. (2004). Radial glia serve as neuronal progenitors in all regions of the central nervous system. Neuron *41*, 881–890.

Audesse, A.J., Dhakal, S., Hassell, L.A., Gardell, Z., Nemtsova, Y., and Webb, A.E. (2019). FOXO3 directly regulates an autophagy network to functionally regulate proteostasis in adult neural stem cells. PLoS Genet. *15*, e1008097.

Bond, A.M., Ming, G.L., and Song, H. (2015). Adult mammalian neural stem cells and neurogenesis: five decades later. Cell Stem Cell *17*, 385–395.

Cameron, B.D., Traver, G., Roland, J.T., Brockman, A.A., Dean, D., Johnson, L., Boyd, K., Ihrie, R.A., and Freeman, M.L. (2019). Bcl2-expressing quiescent type B neural stem cells in the ventricular-subventricular zone are resistant to concurrent temozolomide/X-irradiation. Stem Cell. *37*, 1629–1639.

Cavallucci, V., Fidaleo, M., and Pani, G. (2016). Neural stem cells and nutrients: poised between quiescence and exhaustion. Trends Endocrinol. Metab. *27*, 756–769.

Chavali, M., Klingener, M., Kokkosis, A.G., Garkun, Y., Felong, S., Maffei, A., and Aguirre, A. (2018). Non-canonical Wnt signaling regulates neural stem cell quiescence during homeostasis and after demyelination. Nat. Commun. *9*, 36.

Choi, S.H., Bylykbashi, E., Chatila, Z.K., Lee, S.W., Pulli, B., Clemenson, G.D., Kim, E., Rompala, A., Oram, M.K., Asselin, C., et al. (2018). Combined adult neurogenesis and BDNF mimic exercise effects on cognition in an Alzheimer's mouse model. Science *361*, eaan8821.

Dai, L., Ye, S., Li, H.W., Chen, D.F., Wang, H.L., Jia, S.N., Lin, C., Yang, J.S., Yang, F., Nagasawa, H., and Yang, W.J. (2017). SETD4 regulates cell quiescence and catalyzes the trimethylation of H4K20 during diapause formation in Artemia. Mol. Cell Biol. *37*, e00453-16.

Delgado, A.C., Maldonado-Soto, A.R., Silva-Vargas, V., Mizrak, D., von Känel, T., Tan, K.R., Paul, A., Madar, A., Cuervo, H., Kitajewski, J., et al. (2021). Release of stem cells from quiescence reveals gliogenic domains in the adult mouse brain. Science *372*, 1205–1209.

Doetsch, F., Caillé, I., Lim, D.A., García-Verdugo, J.M., and Alvarez-Buylla, A. (1999). Subventricular zone astrocytes are neural stem cells in the adult mammalian brain. Cell *97*, 703–716.

Engler, A., Rolando, C., Giachino, C., Saotome, I., Erni, A., Brien, C., Zhang, R., Zimber-Strobl, U., Radtke, F., Artavanis-Tsakonas, S., et al. (2018). Notch2 signaling maintains NSC quiescence in the murine ventricular-subventricular zone. Cell Rep. *22*, 992–1002.

Faiz, M., Sachewsky, N., Gascón, S., Bang, K.W.A., Morshead, C.M., and Nagy, A. (2015). Adult neural stem cells from the subventricular zone give rise to reactive astrocytes in the cortex after stroke. Cell Stem Cell *17*, 624–634.

Faria, J.A.Q.A., Corrêa, N.C.R., de Andrade, C., de Angelis Campos, A.C., dos Santos Samuel de Almeida, R., Rodrigues, T.S., de Goes, A.M., Gomes, D.A., and Silva, F.P. (2013). SET domain-containing protein 4 (SETD4) is a newly identified cytosolic and nuclear lysine methyltransferase involved in breast cancer cell proliferation. J. Cancer Sci. Ther. *5*, 58–65.

Fuentealba, L.C., Rompani, S.B., Parraguez, J.I., Obernier, K., Romero, R., Cepko, C.L., and Alvarez-Buylla, A. (2015). Embryonic origin of postnatal neural stem cells. Cell *161*, 1644–1655.

Furutachi, S., Miya, H., Watanabe, T., Kawai, H., Yamasaki, N., Harada, Y., Imayoshi, I., Nelson, M., Nakayama, K.I., Hirabayashi, Y., and Gotoh, Y. (2015). Slowly dividing neural progenitors are an embryonic origin of adult neural stem cells. Nat. Neurosci. *18*, 657–665.

Ganapathi, M., Boles, N.C., Charniga, C., Lotz, S., Campbell, M., Temple, S., and Morse, R.H. (2018). Effect of Bmi1 over-expression on gene expression in adult and embryonic murine neural stem cells. Sci. Rep. *8*, 7464.

Götz, M., and Huttner, W.B. (2005). The cell biology of neurogenesis. Nat. Rev. Mol. Cell Biol. *6*, 777–788.

Hu, X.L., Chen, G., Zhang, S., Zheng, J., Wu, J., Bai, Q.R., Wang, Y., Li, J., Wang, H., Feng, H., et al. (2017). Persistent expression of vcam1 in radial glial cells is required for the embryonic origin of postnatal neural stem cells. Neuron *95*, 309–325.e6.

Kalamakis, G., Brüne, D., Ravichandran, S., Bolz, J., Fan, W., Ziebell, F., Stiehl, T., Catalá-Martinez, F., Kupke, J., Zhao, S., et al. (2019). Quiescence modulates stem cell maintenance and regenerative capacity in the aging brain. Cell *176*, 1407–1419.e14.

Kandasamy, M., Lehner, B., Kraus, S., Sander, P.R., Marschallinger, J., Rivera, F.J., Trümbach, D., Ueberham, U., Reitsamer, H.A., Strauss, O., et al. (2014). TGF-beta signaling in the adult neurogenic niche promotes stem cell quiescence as well as generation of new neurons. J. Cell Mol. Med. *18*, 1444–1459.

Kippin, T.E., Martens, D.J., and van der Kooy, D. (2005). p21 loss compromises the relative quiescence of forebrain stem cell proliferation leading to exhaustion of their proliferation capacity. Genes Dev. *19*, 756–767.

Knobloch, M., Pilz, G.A., Ghesquière, B., Kovacs, W.J., Wegleiter, T., Moore, D.L., Hruzova, M., Zamboni, N., Carmeliet, P., and Jessberger, S. (2017). A fatty acid oxidation-dependent metabolic shift regulates adult neural stem cell activity. Cell Rep. *20*, 2144–2155.

Kriegstein, A., and Alvarezbuylla, A. (2009). The glial nature of embryonic and adult neural stem cells. Annu. Rev. Neurosci. *32*, 149–184.

Kriegstein, A.R., and Götz, M. (2003). Radial glia diversity: a matter of cell fate. Glia *43*, 37–43.

Liao, X., Wu, C., Shao, Z., Zhang, S., Zou, Y., Wang, K., Ha, Y., Xing, J., Zheng, A., Shen, Z., et al. (2021). SETD4 in the proliferation, migration, angiogenesis, myogenic differentiation and genomic methylation of bone marrow mesenchymal stem cells. Stem Cell Rev. Rep. *17*, 1374–1389.

Lim, D.A., and Alvarez-Buylla, A. (2016). The adult ventricular–subventricular zone (V-SVZ) and olfactory bulb (OB) neurogenesis. Cold Spring Harb. Perspect. Biol. *8*, a018820.

Llorens-Bobadilla, E., Zhao, S., Baser, A., Saiz-Castro, G., Zwadlo, K., and Martin-Villalba, A. (2015). Single-cell transcriptomics reveals a population of dormant neural stem cells that become activated upon brain injury. Cell Stem Cell *17*, 329–340.

Lugert, S., Basak, O., Knuckles, P., Haussler, U., Fabel, K., Götz, M., Haas, C.A., Kempermann, G., Taylor, V., and Giachino, C. (2010). Quiescent and active hippocampal neural stem cells with distinct morphologies respond selectively to physiological and pathological stimuli and aging. Cell Stem Cell *6*, 445–456.

Marqués-Torrejón, M.Á., Williams, C.A.C., Southgate, B., Alfazema, N., Clements, M.P., Garcia-Diaz, C., Blin, C., Arranz-Emparan, N., Fraser, J., Gammoh, N., et al. (2021). LRIG1 is a gatekeeper to exit from quiescence in adult neural stem cells. Nat. Commun. *12*, 2594.

Merkle, F.T., Tramontin, A.D., García-Verdugo, J.M., and Alvarez-Buylla, A. (2004). Radial glia give rise to adult neural stem cells in the subventricular zone. Proc. Natl. Acad. Sci. USA *101*, 17528–17532.

Ming, G.L., and Song, H. (2011). Adult neurogenesis in the mammalian brain: significant answers and significant questions. Neuron *70*, 687–702.

Mirzadeh, Z., Merkle, F.T., Soriano-Navarro, M., Garcia-Verdugo, J.M., and Alvarez-Buylla, A. (2008). Neural stem cells confer unique pinwheel architecture to the ventricular surface in neurogenic regions of the adult brain. Cell Stem Cell *3*, 265–278.

Mobley, A.S., Rodriguez-Gil, D.J., Imamura, F., and Greer, C.A. (2014). Aging in the olfactory system. Trends Neurosci. *37*, 77–84.

Obernier, K., and Alvarez-Buylla, A. (2019). Neural stem cells: origin, heterogeneity and regulation in the adult mammalian brain. Development *146*, dev156059.

Ohtsuka, T., and Kageyama, R. (2021). Hes1 overexpression leads to expansion of embryonic neural stem cell pool and stem cell reservoir in the postnatal brain. Development *148*, 189191.

Otsuki, L., and Brand, A.H. (2020). Quiescent neural stem cells for brain repair and regeneration: lessons from model systems. Trends Neurosci. *43*, 213–226.

Prozorovski, T., Schulze-Topphoff, U., Glumm, R., Baumgart, J., Schröter, F., Ninnemann, O., Siegert, E., Bendix, I., Brüstle, O., Nitsch, R., et al. (2008). Sirt1 contributes critically to the redox-dependent fate of neural progenitors. Nat. Cell Biol. *10*, 385–394.

Seri, B., García-Verdugo, J.M., Mcewen, B.S., and Alvarez-Buylla, A. (2001). Astrocytes give rise to new neurons in the adult mammalian Hippocampus. J. Neurosci. *21*, 7153–7160.

Shi, Z., Geng, Y., Liu, J., Zhang, H., Zhou, L., Lin, Q., Yu, J., Zhang, K., Liu, J., Gao, X., et al. (2018). Single-cell transcriptomics reveals gene signatures and alterations associated with aging in distinct neural stem/progenitor cell subpopulations. Protein Cell *9*, 351–364.

Signer, R.A.J., and Morrison, S.J. (2013). Mechanisms that regulate stem cell aging and life span. Cell Stem Cell *12*, 152–165.

Sueda, R., Imayoshi, I., Harima, Y., and Kageyama, R. (2019). High Hes1 expression and resultant Ascl1 suppression regulate quiescent vs. active neural stem cells in the adult mouse brain. Genes Dev. *33*, 511–523.

Urbán, N., Blomfield, I.M., and Guillemot, F. (2019). Quiescence of adult mammalian neural stem cells: a highly regulated rest. Neuron *104*, 834–848.

Xing, S., Tian, J.Z., Yang, S.H., Huang, X.T., Ding, Y.F., Lu, Q.Y., Yang, J.S., and Yang, W.J. (2021). Setd4 controlled quiescent c-Kit^{+} cells contribute to cardiac neovascularization of capillaries beyond activation. Sci. Rep. *11*, 11603.

Yao, B., Christian, K.M., He, C., Jin, P., Ming, G.L., and Song, H. (2016). Epigenetic mechanisms in neurogenesis. Nat. Rev. Neurosci. *17*, 537–549.

Ye, S., Ding, Y.F., Jia, W.H., Liu, X.L., Feng, J.Y., Zhu, Q., Cai, S.L., Yang, Y.S., Lu, Q.Y., Huang, X.T., et al. (2019). SET domain-containing protein 4 epigenetically controls breast cancer stem cell quiescence. Cancer Res. *79*, 4729–4743.